Available online at www.sciencedirect.com

ScienceDirect

Solar Energy 123 (2016) 57–73

SOLAR ENERGY

www.elsevier.com/locate/solener

Critical limitations on the efficiency of two-step thermochemical cycles

Colby Jarrett [a], William Chueh [b], Cansheng Yuan [a,c], Yoshiaki Kawajiri [c], Kenneth H. Sandhage [d,e], Asegun Henry [a,d,*]

[a] George W. Woodruff School of Mechanical Engineering, Georgia Institute of Technology, United States
[b] Department of Material Science and Engineering, Stanford University, United States
[c] School of Chemical & Biomolecular Engineering, Georgia Institute of Technology, United States
[d] School of Materials Science and Engineering, Georgia Institute of Technology, United States
[e] School of Materials Engineering, Purdue University, United States

Received 24 July 2015; received in revised form 23 September 2015; accepted 24 September 2015

Communicated by: Associate Editor Michael Epstein

Abstract

Previous models based on thermodynamic considerations have identified the properties desired for reactive oxides that can be used as oxygen storage materials in thermochemical cycles to produce fuel from sunlight. However, there are several important assumptions made in such models, such as the neglect of the energy required to preheat unreacted species and the assumption of constant vacuum pump efficiency. When these assumptions are relaxed, one comes to significantly different conclusions about the optimal reactor operating conditions. Furthermore, comparing two materials is not straightforward due to the high degree of coupling between material properties and reactor operating conditions. Herein, we describe a new framework for material comparison which employs a thermodynamic reactor model to predict the maximum possible efficiency of a given oxygen storage material. This model demonstrates how new materials can impact reactor performance and the limitations of such improvements.

Keywords: Solar fuels; Thermochemical; Thermodynamic efficiency analysis; Ceria; Hydrogen production; Chemical conversion

1. Introduction

Global warming, pollution, and diminishing reserves are all issues associated with energy derived from fossil fuels. These issues make the development of a clean, sustainable energy infrastructure an imminent, albeit difficult technological challenge (IEA, 2013; Chaisson, 2008; Aleklett et al., 2010; Ngoh and Njomo, 2012; Holladay et al., 2009). Although global energy consumption continues to grow, it is still several orders of magnitude less than the energy received by the earth through solar radiation (Chueh and Haile, 1923). Photovoltaics and concentrated solar thermal power are becoming more established technologies for grid electricity production, but the challenge of finding a path to a renewable and dispatchable fuel for the transportation sector remains a daunting challenge. One promising approach is to store the sun's energy chemically by splitting water to produce hydrogen, which would serve as a dispatchable fuel or fuel precursor. A version of this process, termed thermolysis, can be achieved through the direct splitting of water molecules:

$$H_2O \rightarrow H_2 + \frac{1}{2}O_2 \tag{1}$$

* Corresponding author at: George W. Woodruff School of Mechanical Engineering, Georgia Institute of Technology, United States.
E-mail address: ase@gatech.edu (A. Henry).

http://dx.doi.org/10.1016/j.solener.2015.09.036
0038-092X/

Nomenclature

Abbreviations

OSM	oxygen storage material
NRC	nonstoichiometric redox cycle
P_{O_2}	oxygen partial pressure
W_{Pump}	work to drive vacuum pump
T_H	reduction temperature
T_L	oxidation temperature
Q_{Total}	total energy input to system
Q_{Reheat}	energy needed to heat from T_L to T_H
Q_{RXN}	energy of endothermic reduction reaction
Q_{Water}	energy needed to generate steam
Q_{Out}	energy removed when cooling from T_H to T_L
ε_S	efficiency of solid phase heat recovery
ε_G	efficiency of gas phase heat recovery
Δt	cycle time
$\dot{Q}_{Loss}$	heat leak rate from the system
$M_xO_{y-\delta}$	metal oxide OSM
δ	off-stoichiometry of OSM
δ_O	off-stoichiometry of OSM after oxidation
δ_R	off-stoichiometry of OSM after reduction
n_{H_2O}	moles of water needed for oxidation per cycle
HHV_{H_2}	higher heating value of hydrogen
LHV_{H_2}	lower heating value of hydrogen
C_P^{OSM}	molar specific heat of the OSM
$C_P^{H_2O}$	molar specific heat of water
ΔH	change in enthalpy upon reduction
ΔS	change in entropy upon reduction
η	NRC chemical conversion efficiency
F_{Reheat}	energy factor for temperature change
F_{RXN}	energy factor for endothermic reduction
F_{Water}	energy factor for generating steam
F_{Pump}	energy factor for driving the vacuum pump
F_{Loss}	energy factor for heat leak
R_{TM}	ratio of inert reactor thermal mass to OSM thermal mass
$\dot{Q}_{Re\text{-}Rad}$	heat leak rate from re-radiation at the solar receiver
C_{H_2O}	extent of chemical conversion (ratio of water to hydrogen)
R_{H_2O}	ratio of water to hydrogen at reactor outlet during oxidation
K_{WS}	chemical equilibrium constant for water dissociation
$R_{\Delta H}$	ratio of ΔH to the change in enthalpy of water dissociation
η_{Pump}	efficiency of vacuum pump
T^o	reference temperature
P^o	reference pressure
R	gas constant
W_{Pump}^{Ideal}	ideal pump work
$W_{Friction}$	lost frictional work of vacuum pump
ΔH_{H_2O}	enthalpy of liquid water dissociation

Such a direct process has high theoretical efficiencies, but the requirement of temperatures above 2500 K (with gaseous product separations) limits its feasibility (Steinfeld, 2005). These two issues can be addressed by dividing the process into two or more separate reaction steps where the net reaction is water dissociation.

Hundreds of thermochemical cycles with varying numbers of reaction steps have been proposed and investigated for water splitting (Funk, 2001; Abanades et al., 2006; Funk and Reinstro, 1966). Among the most promising of these are two-step redox cycles, due to their simplicity and high theoretical efficiency (Steinfeld, 2005). A schematic illustration of a thermochemical two-step metal oxide redox cycle, revealing the relevant energy and mass balances, is shown in Fig. 1. Here, an intermediate oxygen storage material (OSM), such as a metal oxide, is first reduced at a high temperature, T_H (via Reaction (2)). The OSM is then cooled to a lower temperature, T_L, where it then re-oxidizes when exposed to steam (via Reaction (3)).

In the indicated cycle, a vacuum pump can be used to reduce the total pressure and oxygen partial pressure (P_{O_2}) to allow for the reduction of an OSM (Ermanoski et al., 2014; Venstrom et al., 2014). The energy input to the system includes the work needed to drive the vacuum pump (W_{Pump}), the sensible heat needed to raise the temperature of the reactor and OSM from T_L to T_H (Q_{Reheat}), the energy needed to drive the endothermic reduction reaction (Q_{RXN}), along with the sensible and latent heat associated with generating the reactant steam (Q_{Water}). Note that by carrying out heat recuperation, some portion of the sensible heat removed from the reactor (Q_{Out}) and some portion of the sensible heat removed from the product stream during step two ($H_2 + H_2O$) can be recovered at an efficiency of ε_S and ε_G respectively. During the time required to complete both steps of the reaction (Δt), heat leaks from the system to the environment at a rate of $\dot{Q}_{Loss}$.

For the metal oxide ($M_xO_{y\text{-}\delta}$), δ_R and δ_O represent the off-stoichiometry (oxidation state) after steps one and two respectively. In Reaction (3), n_{H_2O} is the number of moles of water required to oxidize one mole of OSM from δ_R to δ_O at T_L. The units of $\delta_R - \delta_O$ can be taken as the moles of hydrogen produced per mole of OSM per cycle. For a two-step cycle, the OSM can be a pure or alloyed material undergoing partial reduction, or an arbitrary number of intermediate compounds or solution phases that absorb and release oxygen through reversible reactions (Meredig and Wolverton, 2011). Conceptually, one could

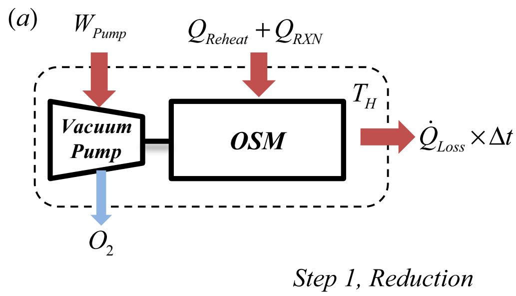

$$M_xO_{y-\delta_O} \rightarrow M_xO_{y-\delta_R} + \frac{\delta_R - \delta_O}{2} O_2 \quad (2)$$

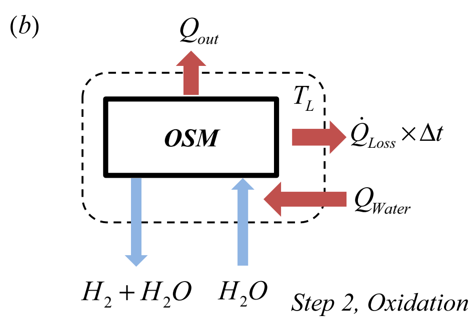

$$M_xO_{y-\delta_R} + n_{H_2O}H_2O \rightarrow M_xO_{y-\delta_O} + (\delta_R - \delta_O)H_2 + \{n_{H_2O} - (\delta_R - \delta_O)\}H_2O \quad (3)$$

Fig. 1. Schematic of energy and mass transfers in a two-step thermochemical redox reactor, (a) reduction, (b) oxidation. Q_{Reheat}, Q_{RXN}, and Q_{Out} refer to the sensible heat need to raise the OSM temperature, to drive the endothermic reduction reaction, and that is removed upon cooling of the OSM, respectively. It should also be noted that the exothermic heat released by the OSM upon reoxidation is included in Q_{Out} and can be used to preheat the inlet steam. W_{Pump} is the work needed to drive the vacuum pump, and $Q_{\mathrm{Loss}} \times \Delta t$ is the sensible heat that is assumed to leak from the system each reaction cycle.

also design a two-step cycle based on a hydrogen storage material. However, many metal hydrides lack the necessary high temperature stability to facilitate efficient water splitting. While new metal hydrides are certainly worthy of future materials exploration, we will herein focus specifically on metal oxides. The framework presented herein could easily be extended to hydrides if so desired.

While the OSM completely reduces for some cycles ($y = \delta_R$) (Loutzenhiser and Steinfeld, 2011) Reactions (2) and (3) represent a nonstoichiometric redox cycle (NRC) where the OSM is only partially reduced and/or oxidized respectively. One of the principle advantages of NRCs is their potential for high cyclability with low OSM degradation, since they retain the same crystallographic phase. For each step of a NRC, the equilibrium non-stoichiometry δ can be found from the thermochemical properties of the OSM, temperature (T), and oxygen partial pressure (P_{O_2}) through the following relation (Scheffe and Steinfeld, 2012):

$$\Delta H(\delta) - T\Delta S(\delta) = -RT \ln(P_{O_2}) \quad (4)$$

Here $\Delta H(\delta)$ and $\Delta S(\delta)$ are the standard enthalpy and entropy changes of the OSM associated with the loss of oxygen. The values of these enthalpy and entropy changes are generally functions of δ and for some materials also exhibit significant variation with temperature.

Cerium dioxide (ceria, CeO_2) has received increased attention in recent years as an OSM for NRCs, primarily due to the low volatility of its reduced state ($CeO_{2-\delta}$), fast oxidation kinetics, and extended cycle durability (Chueh and Haile, 1923). Other promising materials include transition metal perovskite oxides (Scheffe et al., 2013; McDaniel et al., 2013) and ferrites (Scheffe et al., 2010) which can achieve relatively high extents of reduction, thereby yielding more hydrogen per cycle than ceria.

As new materials are developed, it is important to establish a framework for evaluating the extent to which such materials can actually improve the system level NRC efficiency. In the present paper, a general framework is developed that allows for the optimization of NRC efficiency by simultaneous consideration of OSM properties and operating conditions of the thermochemical two-step redox. Such a framework is needed because one cannot define a figure of merit or assess an OSM's efficiency solely from its material properties, without describing the reactor in which it is used. Thus, it becomes difficult to determine if a given OSM has the ability to enable higher system efficiencies than another, without also considering the reactors. As a result, the purpose of the framework presented herein is to aid in the identification and engineering of the optimal material, since at present it is not clear what properties the optimal material would ideally or realistically have. Using ceria as the base-case OSM, we explore the potential for improvement via alternative OSMs and identify two critical system energy inputs W_{Pump} and Q_{Water}. These inputs have been considered previously (Bulfin et al., 2015; Brendelberger et al., 2014), but here we integrate them into a more general framework that allows one to determine the highest possible efficiency that can be obtained for a given OSM. Such an analysis is quite complicated and somewhat daunting, considering that there are a myriad of reactor level parameters that can affect the ultimate system efficiency. However, here we have taken up the task of attempting to distil the problem down to its most fundamental limitations, whereby we identify two important critical limitations that do not appear to be surmountable. To reach this point, the forthcoming thermodynamic efficiency analysis examines each parameter that can affect the efficiency to determine what its fundamental and practical limitations are. We then consider the limiting case where each parameter takes on the value that yields the highest efficiency, subject to its fundamental and practical limits. This choice of parameters then allows one to determine the highest possible efficiency that can be achieved with a given OSM. Once established, the modelling framework described herein then allows one to

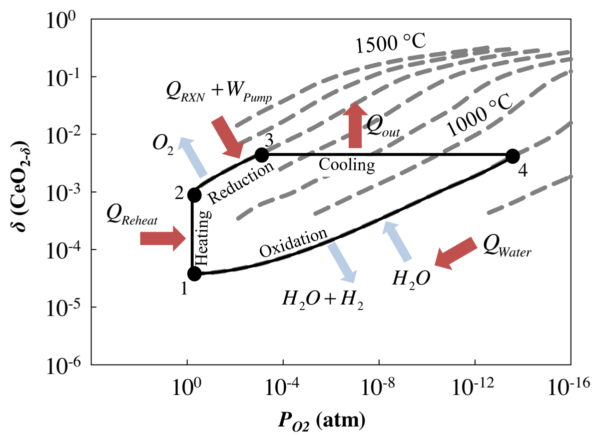

Fig. 2. Equilibrium oxygen off-stoichiometry (δ) of ceria vs. P_{O_2}. Isotherms (dotted lines) are shown in 100 °C increments for temperatures in the range of in 800–1500 °C (Panhans and Blumenthal, 1993). The states the OSM traverses for an idealized two-step NRC ($T_H = 1300$ °C, $T_L = 800$ °C, $P_{O_2} = 10^{-3}$ atm, and $\delta_O = 0.0025$) are superimposed on this plot (solid lines). The OSM is heated from 800 °C to 1300 °C (points 1 → 2), then it is reduced at 1300 °C (points 2 → 3), then it is cooled from 1300 °C to 800 °C (points 3 → 4), and finally oxidized at 800 °C (points 4 → 1).

examine how sensitive the efficiency is to various parameters and a variety of example cases are discussed to highlight that the choice of OSM can significantly change how a reactor should be cycled so as to reach maximum efficiency. Example cases are then used to better illustrate how this more general framework can guide the design and set the priorities for future OSM and reactor engineering.

2. Energy factors affecting NRC efficiency

The thermal efficiency (η) of a NRC is given as (Steinfeld, 2005),

$$\eta = \frac{n_{H_2} \times \mathrm{HHV}_{H_2}}{Q_{\mathrm{Total}}} \tag{5}$$

where,

$$Q_{\mathrm{Total}} = Q_{\mathrm{Reheat}} + Q_{\mathrm{RXN}} + Q_{\mathrm{Water}} + W_{\mathrm{Pump}} + Q_{\mathrm{Loss}} \tag{6}$$

Note the Q_{Loss} in Eq. (6) includes the portion of Q_{out} in Fig. 1b that is not used to preheat reactants. In Eq. (5) n_{H_2} is the number moles of hydrogen produced per cycle ($\delta_R - \delta_O$), HHV_{H_2} is the higher heating value of hydrogen, and Q_{Total} is the total energy input per cycle. All energy inputs in Eq. (6) are heat contributions except for the work required to pump all fluids and most critically the vacuum pump, if used to drive the reduction. If converted to a heat input, an additional efficiency penalty exists, associated with converting heat to work. However, as will be shown in the ensuing analysis, this additional factor is of minimal consequence because the pumping power for a vacuum pump changes by many orders of magnitude. Thus, a factor of 2-3X higher energy requirement associated with the heat needed to generate the work would not qualitatively alter the ultimate conclusions.

Thermochemical reactors are inherently complex systems. Fluid mechanics, chemical reactions, heat transfer, mass transfer, as well as their coupling, must be considered in order to model the reactor efficiency. Additionally, the design space for the reactor parameters (such as T_H, T_L, and P_{O_2}) and the range of options for the OSM are large. Hence, it is difficult to develop a single all-encompassing model for efficiency and OSM performance (Ermanoski et al., 2014; Siegel et al., 2013; Krenzke and Davidson, 2015; Mallapragada and Agrawal, 2014). Reports on systems where the OSM is restricted to ceria can be found by Lapp et al. (2012), Siegel et al. (2013), and Ermanoski et al. (2013). Parameters that affect efficiency include operational and design parameters such as heat recovery, the inert thermal mass of the reactor, T_H, T_L, as well as material parameters, such as: specific heat of the OSM (C_P), ΔH and ΔS of reduction, and the extent of oxidation (δ_O). The extent of reduction, δ_R, is determined from OSM material properties, T_H, and P_{O_2}. To better understand the complex relationship between these parameters and performance, it is convenient to express the efficiency in terms of dimensionless energy factors (Eq. (7)), where each factor represents a particular required energy input of the cycle (shown in Fig. 1) normalized by the output energy stored chemically in hydrogen, as follows:

$$\eta = \frac{1}{F_{\mathrm{Reheat}} + F_{\mathrm{RXN}} + F_{\mathrm{Water}} + F_{\mathrm{Pump}} + F_{\mathrm{Loss}}} \tag{7}$$

where F_{Reheat}, F_{RXN}, F_{Water}, F_{Pump}, and F_{Loss} are the energy factors associated with heating the OSM, driving the endothermic reduction reaction, producing steam, driving the vacuum pump, and heat leakage from the system, respectively. Eqs. (8)–(12) define the energy factors used in Eq. (7). By evaluating the relative magnitudes of each factor, one can identify which energy inputs dominate and the parameters that govern the dominant inputs can provide insight into potential directions for improvement.

F_{Reheat}, which accounts for the sensible energy required to heat the OSM and inert reactor components from T_L to T_H (Fig. 2, points 1 → 2), is modelled as follows:

$$F_{\mathrm{Reheat}} = \frac{Q_{\mathrm{Reheat}}}{n_{H_2} \times \mathrm{HHV}_{H_2}} = \frac{(1-\varepsilon_S)\int_{T_L}^{T_H} (R_{\mathrm{TM}}+1) C_P^{\mathrm{OSM}} dT}{(\delta_R - \delta_O) \times \mathrm{HHV}_{H_2}} \tag{8}$$

where ε_S is the fraction of solid phase heat that is recovered upon cooling (points 3 → 4), R_{TM} is the ratio of inert reactor thermal mass to OSM thermal mass, and C_P is the specific heat of the OSM.

F_{RXN}, which represents the energy required to liberate oxygen during the endothermic reduction reaction relative to the energy stored chemically in hydrogen (points 2 → 3), is modelled as:

$$F_{\mathrm{RXN}} = \frac{Q_{\mathrm{RXN}}}{n_{H_2} \times \mathrm{HHV}_{H_2}} = \frac{\Delta H}{\mathrm{HHV}_{H_2}} \tag{9}$$

F_{Water}, which accounts for the sensible heat needed to vaporize and preheat water used to oxidize the OSM (Fig. 2, 4 → 1), is modelled as:

$$F_{\text{Water}} = \frac{Q_{\text{Water}}}{n_{H_2} \times \text{HHV}_{H_2}} = \frac{(1-\varepsilon_G)\left\{n_{H_2O}\int_{T^o}^{T_L} C_P^{H_2O}dT - (\Delta H - \text{LHV}_{H_2})\right\}}{(\delta_R - \delta_O) \times \text{HHV}_{H_2}} \quad (10)$$

where ε_G is the fraction of gas phase heat that is recovered, C_P is the specific heat of water, and T^o is the ambient temperature of the reactants fed into the system. Here, the difference between ΔH and the LHV_{H_2} accounts for the exothermic energy released during oxidation that can be utilized to preheat water. If this term is greater than or equal to the energetic expense of heating water, then the excess exothermic energy can be rejected from the system (wasted) and F_{Water} becomes zero.

F_{Pump}, which accounts for the energy required to produce the low P_{O_2} atmosphere during reduction (2 → 3), is modelled as:

$$F_{\text{Pump}} = \frac{W_{\text{Pump}}}{n_{H_2} \times \text{HHV}_{H_2}} = \frac{W_{\text{Pump}}}{(\delta_R - \delta_O) \times \text{HHV}_{H_2}} \quad (11)$$

For OSMs and reduction temperatures that require a P_{O_2} less than 0.21 atm, W_{Pump} is the work required to drive the vacuum pump used to reduce the pressure to the desired P_{O_2}.

Finally, F_{Loss}, which accounts for the heat leakage in the system (where Δt is the time required to complete one reaction cycle), is expressed as:

$$F_{\text{Loss}} = \frac{Q_{\text{Loss}}}{n_{H_2} \times \text{HHV}_{H_2}} = \frac{(\dot{Q}_{\text{Loss}}) \times \Delta t}{(\delta_R - \delta_O) \times \text{HHV}_{H_2}} \quad (12)$$

As defined here, the thermochemical conversion efficiency (η) only describes the reactor's ability to convert thermal energy to chemical energy; that is, losses associated with converting sunlight to thermal energy are ignored. Therefore, in Eq. (12), $\dot{Q}_{\text{Loss}}$ represents the heat leakage from the reactor and does not include heat losses associated with converting sunlight to heat (e.g., such as re-radiation losses), which are known to limit the performance of current systems (Keene et al., 2013).

Presumably, a thermochemical reactor would receive its heat input from solar energy, thereby allowing for clean renewable fuel generation. However, the details of how the heat is provided to the reactor are ignored here in favor of finding an upper limiting efficiency for a given OSM. This choice is motivated by the fact that the efficiency of converting sunlight into heat is only fundamentally limited by the extent to which one can concentrate sunlight terrestrially. This limit, however, is extremely high (>46,000 suns) with a high index material (Gleckman et al., 1989) and, thus, it conceivable that one can convert sunlight to heat with >80–90% efficiency. Furthermore, several new reactor designs have now been analyzed that can separate the process of converting sunlight to heat from the conversion of heat to energy stored in chemical bonds (Ermanoski et al., 2013; Yuan et al., 2015a,b; Koepf et al., 2012). Thus, although many current reactor designs perform both conversions in a single device and are typically limited by reradiation losses, this problem is not a true fundamental or practical limitation (Keene et al., 2013). Accordingly, the ensuing analysis focuses specifically on the reactor, so as to examine and identify fundamental/practical limitations associated with the thermo-to-chemical conversion process. As a result, all efficiencies reported herein would be lower, when one accounts for the conversion of sunlight to heat, but the values reported herein represent the intrinsic upper limit associated with the OSM itself.

A quasi-static two-step redox cycle is schematically illustrated by a solid line in Fig. 2. Although this path is not possible in an actual reactor, assuming such an idealized cycle allows an upper bound to be placed on system efficiency. In this figure, the isothermal reduction step (points 2 → 3) and the isothermal oxidation step (points 4 → 1) are assumed to follow the equilibrium relationships between p_{O_2}, T, and δ described by Eq. (4). The heating step (points 1 → 2) is conducted at a constant p_{O_2} and is also assumed to follow the equilibrium relationship of Eq. (4). By assuming the cooling step (points 3 → 4) is conducted at a sufficiently rapid rate as to keep the nonstoichiometry (δ) of the OSM constant, the hydrogen produced per cycle is maximized. This condition determines the upper limit for NRC efficiency.

3. Operational considerations

3.1. Prior work on reactor optimization

The high theoretical efficiencies reported for NRC's (Siegel et al., 2013; Lapp et al., 2012; Ermanoski et al., 2013; Lange et al., 2014) have yet to be realized in experimental reactors (Chueh and Haile, 1923; Furler et al., 2013). In previous experimental reactors, the T_H was achieved by heating via direct solar irradiation. Keene et al. (2013) showed that the low efficiencies observed in such systems are primarily caused by massive heat losses associated with re-radiation ($\dot{Q}_{\text{Re-rad}}$). However, it is important to recognize that, for the reactor itself, F_{Loss} is the only energy factor which is proportional to cycle time. Therefore minimization of heat losses and increasing power density are the only motivations for lowering Δt, (i.e., fast thermal cycling and reaction kinetics). All other energy factors are essentially rate independent.

Ermanoski et al. (2013) reported on a moving packed bed reactor concept that decoupled the fuel production rate from the incoming solar flux. This design allowed the fuel production rate to be tuned, minimizing F_{Loss}. Furthermore, Lapp and Lipiński (2014) reported on a counter-rotating reactor with a value of ε_S that is larger than 50%

for temperature swings greater than 400 °C. More recently Yuan et al. have reported a reactor design that uses liquid metal as an intermediate heat transfer fluid and, based on their modelling results, can enable high recuperation efficiencies >80% (Yuan et al., 2015a,b). Their design (Yuan et al., 2015a,b) also claims to enable efficiencies ~20% for the thermal-to-chemical conversion.

Although reactor designs are improving and re-radiation losses are decreasing, the optimization of thermochemical conversion efficiency remains an important issue that continues to be extensively studied (Siegel et al., 2013; Lapp et al., 2012; Ermanoski et al., 2013; Lapp and Lipiński, 2014; Bader et al., 2013). For these studies, the reactor, operating conditions, and modelling methods vary. Nonetheless, there have been three primary pathways identified for future improvement. First, due to the large thermal load required to swing the OSM temperature from T_L to T_H, recovering this sensible heat is critical to high performance. This implies that the best reactor serves as an effective heat exchanger that achieves the conditions required to make each reaction thermodynamically favorable with minimal losses. Hence, increased performance could come from reactors with better heat recovery. Second, in the limit of a perfect reactor where $\varepsilon_s = 1$, $\varepsilon_G = 1$, and W_{Pump} and Q_{Loss} are negligible, the maximum theoretical efficiency is the inverse of F_{RXN}. Decreasing ΔH therefore decreases this energy factor, which serves as a fundamental limiting efficiency for the OSM itself. Furthermore, as ΔH decreases, the OSM can achieve deeper reductions and δ_R increases. With δ_O fixed, larger δ_R reduces all other energy factors (except F_{RXN}). Thus, the discovery of a new OSM with a lower value of ΔH could improve cycle efficiency. Third, as the energy required to drive a vacuum has been shown to be small relative to the energy stored chemically in hydrogen, operating reactors at the lowest possible pressure should result in high efficiencies (Ermanoski et al., 2013) by increasing δ_R. With these basic insights in mind, we now examine more deeply two critical issues, which are fundamentally limiting and, therefore, introduce important tradeoffs in the reactor efficiency.

3.2. Importance of OSM reduction enthalpy change and the extent of chemical conversion

The extent of chemical conversion describes the fraction of a reactant that is converted into reaction products. This important quantity is of interest because it determines the thermal load required to preheat the water used during oxidation ($n_{\mathrm{H_2O}}$) from T^o to T_L. We define the extent of chemical conversion of steam during the OSM oxidation of a step two NRC as follows:

$$C_{\mathrm{H_2O}} = 1 - \frac{n_{\mathrm{H_2O}} - (\delta_R - \delta_O)}{n_{\mathrm{H_2O}}} = \frac{n_{\mathrm{H_2}}}{n_{\mathrm{H_2O}}} \tag{13}$$

The ratio of unreacted steam to hydrogen in the product stream, $R_{\mathrm{H_2O}}$, is then defined as:

$$R_{\mathrm{H_2O}} = \frac{1}{C_{\mathrm{H_2O}}} - 1 \tag{14}$$

Generally, increasing $C_{\mathrm{H_2O}}$ lowers F_{Water} and increases efficiency. An upper limit for $C_{\mathrm{H_2O}}$ and therefore efficiency can be established by neglecting reaction kinetics. Assuming sufficiently fast reaction kinetics, such that none of the transient behavior is limited by reaction kinetics, is further motivated by the fact that kinetics are not a fundamental limitation. Presumably, if necessary, one could introduce catalysts to increase the reaction rate, but the thermodynamic limitations are insurmountable. Thus, by neglecting any limitations associated with kinetics, the maximum instantaneous conversion can be found from the equilibrium effective $P_{\mathrm{O_2}}$ established by the hydrogen to water ratio at a given value of δ (Fig. 2 and Eq. (4)). With this effective $P_{\mathrm{O_2}}$, the hydrogen to water ratio at the reactor outlet can be found with the following equation,

$$K_{\mathrm{WS}}(T) = P_{\mathrm{O_2}}^{1/2} / R_{\mathrm{H_2O}} \tag{15}$$

where K_{WS} is the equilibrium constant for $H_2O \rightarrow \mathrm{H_2} + 1/2\mathrm{O_2}$. Combining Eqs. (4) and (14), $C_{\mathrm{H_2O}}$ can be written as a function of temperature, ΔH, and ΔS as follows,

$$C_{\mathrm{H_2O}} = \frac{K_{\mathrm{WS}}(T)}{\left(\exp\left(\frac{-(\Delta H(\delta) - T\Delta S(\delta))}{RT}\right)\right)^{1/2} + K_{\mathrm{WS}}(T)} \tag{16}$$

This expression is plotted in Fig. 3 for different values of $R_{\Delta H}$, where $R_{\Delta H}$ defines the ratio of the OSM's ΔH of reduction to $\mathrm{LHV_{H_2}}$ (shown below).

$$R_{\Delta H} = \frac{\Delta H}{\mathrm{LHV_{H_2}}} \tag{17}$$

As a nominal example, Fig. 3 was created using the value of ΔS corresponding to ceria at $\delta = 0.005$. As ΔH is reduced at constant oxidation temperature, $C_{\mathrm{H_2O}}$ also decreases and the hydrogen concentration in the product stream consequently decreases. It is important to note in Fig. 3, that the vertical axis is depicted on a logarithmic

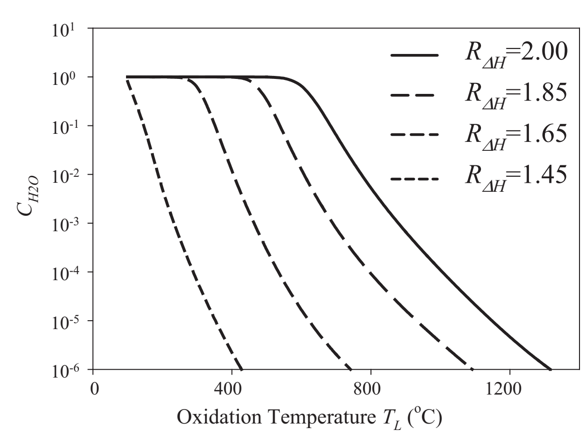

Fig. 3. Fraction of water conversion as defined in Eq. (15) with $\Delta S = 316$ J/K-mol $\mathrm{H_2}$ (here, ΔS is assumed to be that of ceria at $\delta = 0.005$ (Panhans and Blumenthal, 1993). For ceria with $\delta = 0.005$, $R_{\Delta H} = 2.00$.

scale, indicating that the amount of conversion changes by many orders of magnitude with respect to a seemingly small ~10% change in ΔH, for a fixed oxidation temperature. Fundamentally, this is a consequence of the exponential in Eq. (16). Thus, the optimum oxidation temperature and ΔH are highly coupled, as Fig. 3 shows that for low values of ΔH and high T_L, a large amount of unreacted water is required to drive the OSM reoxidation (step 2). Fig. 3 also shows how low conversion can be combatted by decreasing the oxidation temperature; that is lower oxidation temperatures are required for low ΔH materials to reach high efficiency.

The inverse of C_{H_2O} represents the number of moles of water required for oxidation, per mole H_2 produced. The total amount of water required for oxidation can be evaluated from Eq. (18) and can be substituted into Eq. (10) to determine F_{Water}.

$$n_{H_2O} = \int_{\delta_O}^{\delta_R} 1/C_{H_2O} d\delta \tag{18}$$

The experimental equilibrium off-stoichiometry of ceria is shown as a function of P_{O_2} and T (Panhans and Blumenthal, 1993) in Fig. 2. This OSM approaches complete oxidation even at very low values of P_{O_2}, implying that ceria has very high C_{H_2O} over the course of oxidation. This high C_{H_2O} is due to the relativity high ΔH of ceria, which is nearly twice the enthalpy change required for water dissociation (Zinkevich et al., 2006). With T_L held constant, reducing ΔH decreases C_{H_2O} and increases F_{Water}. Thus there is a trade-off associated with smaller ΔH, as lowering ΔH decreases F_{RXN} and increases δ_R, it also increases F_{Water} and/or F_{Reheat}.

Although the relationship between the OSM's ΔH and efficiency is complicated, there are upper and lower limits to the values of ΔH desirable for a NRC. If $R_{\Delta H}$ is less than 1, then the oxidation shown in reaction (3) will be endothermic and the OSM is not likely to have any thermodynamic potential to overcome the modest entropy decrease during OSM oxidation with steam (step 2). On the other hand, if $R_{\Delta H}$ is too large, then the T_H will be prohibitively high and/or the P_{O_2} will be prohibitively low for significant fuel production. For the ensuing discussion, we have assumed the δ and T dependence of ΔH to be that of ceria, to simplify our analysis. However it should be noted, that if the dependence for another OSM is different, then the major qualitative conclusions from the subsequent analysis are likely to be unchanged.

Meredig and Wolverton (2011) mapped ranges of ΔH and ΔS that are viable for thermochemical water splitting by evaluating the ability for water to oxidize a reduced OSM from a thermodynamic perspective. Miller et al. (2014) reviewed the many factors affecting the OSM design including, but not limited to, OSM thermodynamic properties. The authors noted that a maximum theoretical efficiency is achieved at the lowest limit on the value of ΔH (i.e., the enthalpy of water dissociation). However, because the calculations of theoretical efficiency ignore the losses from low C_{H_2O}, this conclusion may not translate to real reactors.

For some OSM's with high C_{H_2O} (ceria), very little unreacted steam flows through the reactor and, therefore, the losses from preheating excess steam are negligible. Detailed system efficiency analyses of NRCs using ceria as the OSM have either neglected these losses ($n_{H_2O} = \delta_R - \delta_O$) (Lapp et al., 2012) or assumed that the losses are fixed and small (3%) (Siegel et al., 2013), which are both valid and good assumptions for ceria. When modelling cycles which use different OSMs with lower ΔH (Scheffe et al., 2013, 2010; McDaniel et al., 2013), however, the lower value of C_{H_2O} could require larger amounts of unreacted water ($n_{H_2O} - (\delta_R - \delta_{OX})$), increasing the energy penalty associated with preheating this excess water (F_{Water}). The goal of the new framework presented herein is to enable evaluation of the efficiencies achievable by different OSMs, while accounting for the coupling between reactor design, operational parameters, and OSM properties.

3.3. The influence of pump efficiency

The P_{O_2} of reaction step 1 (OSM reduction) is commonly reduced to increase the thermodynamic driving force for reduction. Doing so increases δ_R with the aim of achieving higher efficiencies. An inert sweep gas can be used to reduce the P_{O_2}, but this can be energetically expensive (Chueh and Haile, 1923). Therefore, previous work has highlighted the use of a vacuum pump as a more promising means of achieving low P_{O_2} (Siegel et al., 2013; Ermanoski et al., 2013). As a result, attention has shifted to using mechanical vacuum pumping to achieve low pressures, and it has even prompted analysis and testing of isothermal cycles (Bader et al., 2013; Muhich et al., 2013). The minimum possible work required to produce a vacuum can be derived by assuming negligible heat transfer and isothermal compression as:

$$W_{Pump} = \int_{\delta_O}^{\delta_R} \frac{n_{O_2}(\delta)}{\eta_{Pump}(P(\delta, T))} RT^o \ln\left(\frac{P^O}{P_{O_2}(\delta, T)}\right) d\delta \tag{19}$$

where η_{Pump} is the efficiency of the pump, n_{O_2} is the number of moles of oxygen that traverse the pump during reduction, R is the gas constant, T^o is the pump temperature, P^o is the reference pressure on the high pressure side of the vacuum pump, and P_{O_2} is the reduced total pressure and oxygen partial pressure. This expression differs slightly from previous models, which assumed that all of the oxygen (n_{O_2}) was removed at a constant pressure equal to the final reduction pressure (Siegel et al., 2013; Ermanoski et al., 2013). Eq. (19) accounts for the oxygen gas that evolves during the transient reduction of reactor pressure. Here, n_{O_2} is a function of δ and is defined by,

$$n_{O_2} = \frac{(\delta_R - \delta_O)}{2} \tag{20}$$

If one neglects pumping efficiency, W_{Pump} as it is defined in Eq. (19) is always smaller than W_{Pump} as it is defined in previous expressions where P is held constant at the final P_{O_2} (Siegel et al., 2013; Ermanoski et al., 2013) (shown in Eq. (20)). Ermanoski et al. (2013) reported a monotonic relationship between reduction P_{O_2} and reactor efficiency (Ermanoski et al., 2013), but suggested a lower limit for P_{O_2} in the range of 10^{-3}–10^{-4} atm for reactors ranging from 10^2 to 10^3 kW. This limit results from the hardware requirements of pumping large volumes of low density gas. Bulfin and et al. (2015) and Brendelberger et al. (2014) modelled vacuum pump efficiency as pressure dependent, with a power law dependence for pressure. In other analyses, the efficiency of the pump is either neglected or assumed to be on the order of 10% and constant. For example, Ermanoski et al. assumed a vacuum pump efficiency of 40% (Ermanoski et al., 2013). Other methods of reducing the P_{O_2} could also be used (e.g., electrochemical pumps), however, if mechanical vacuum pumps are used, similar to those used in the silicon manufacturing industry, then an estimation of the pump efficiency is straightforward (provided that pump performance data is available).

Different pumping technologies may be required, depending on the desired operating pressures. For higher pressures, a displacement pump is often used to lower the pressure to approximately 10^{-4} atm followed by the use of another pump to reach the final vacuum pressure (e.g., a magnetically-levitated turbo pump). The efficiency of these pumps can be defined as the ideal pump work over the actual electrical power consumption as follows:

$$W^{\mathrm{Ideal}}_{\mathrm{Pump}} = n_{\mathrm{O}_2} R T^o \ln\left(\frac{P^O}{P}\right) \tag{21}$$

$$\eta_{\mathrm{Pump}} = \frac{W^{\mathrm{Ideal}}_{\mathrm{Pump}}}{W_{\mathrm{Electrical}}} = \frac{W^{\mathrm{Ideal}}_{\mathrm{Pump}}}{W^{\mathrm{Ideal}}_{\mathrm{Pump}} + W_{\mathrm{Friction}}} \tag{22}$$

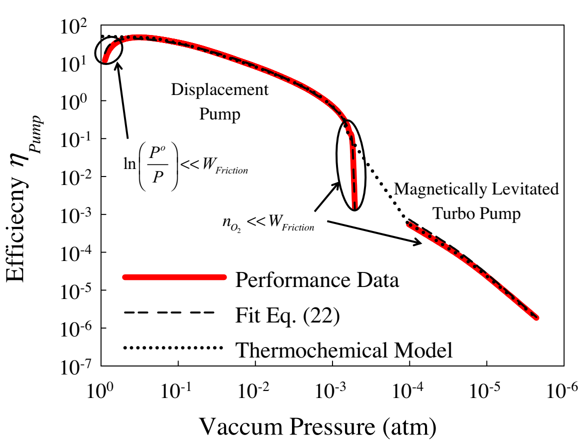

Fig. 4. Efficiency of two example pumps used to achieve medium and low pressures. Performance data was acquired from Becker Pumps Corp. and Turbo Vacuum Pumps for the displacement and turbo pump respectively. The dashed line was obtained by fitting the expression in Eq. (22) to the data provided for each pump. The dotted line shows the values used in the ensuing analysis, whereby the efficiency between 10^{-3} atm and 10^{-4} atm was linearly interpolated between the two data sets (on a log scale).

Fig. 4 shows the efficiency of two commercially-available pumps operating at different vacuum levels. As can be seen in this figure, vacuum pump performance becomes extremely poor at pressures less than 10^{-3} atm. This poor performance can be explained and understood by modelling the pump efficiency using Eq. (22), which is justified by the following rationale. As the pressure decreases, the gas density decreases and the number of gas molecules removed by the pump for each impeller rotation decreases (n_{O_2}). However, the work lost to a small amount of internal friction remains essentially constant as pressure drops. Using the frictional loss as a fitting parameter, Eq. (22) was fit to the performance data and exhibits excellent agreement confirming the validity of the aforementioned explanation (Fig. 4). The exact expressions and pump performance data used to generate the data in Fig. 4 are provided in the supplementary information.

Although vacuum pumps have not been optimized specifically for thermochemical reactors, the efficiency trend shown in Fig. 4 is not likely to change dramatically and therefore order of magnitude efficiency improvements are unlikely. With the aim of accurately predicting the energy required to achieve a low P_{O_2}, the functional dependence of the pump efficiency shown in Fig. 4 was incorporated into Eq. (19) to calculate F_{Pump} in the ensuing analysis (see supplementary information for details).

4. Coupling between material properties and operational parameters

4.1. Efficiency model

For the model of thermochemical conversion efficiency described in Eqs. (4)–(19), the following parameters determine the NRC efficiency,

$$\eta = \eta(\dot{Q}_{\mathrm{Loss}},\ \Delta t, T_H, \varepsilon_G, \varepsilon_S, R_{\mathrm{TM}}, \Delta H(\delta), \Delta S(\delta), C_P^{\mathrm{OSM}},\ T_L,\ P_{\mathrm{O}_2},\ \delta_O) \tag{23}$$

$\dot{Q}_{\mathrm{Loss}}$ is the heat loss rate from the reactor, which is proportional to the reactor's surface area. These losses can be mitigated through reactor design and by minimizing cycle time (Δt). While the kinetics of the OSM oxidation and reduction reactions can determine cycle time, other considerations may also limit the rate at which the reactor can be cycled. Such factors include: the time required to reach the desired P_{O_2} and the time required to change the OSM temperature from T_H to T_L (which can be bounded by thermal shock or heat and mass transport limitations). If temperature swings of more than a few hundred degrees are required, then avoidance of excessive thermal shock may set a lower bound on Δt, on the order of minutes. Since current reactors have exhibited cycle times on the order of tens of minutes, it seems unlikely that more than one order of magnitude decrease in cycle time can be realized without sacrificing long reactor lifetime. In the subsequent analysis, $\dot{Q}_{\mathrm{Loss}}$ and Δt are excluded for simplicity and because as Yuan et al. (2015a) have shown, some reactor designs are scalable in such a way that at large scales this loss can be suppressed to arbitrarily low values simply limited by capital risk. As a result, the remaining efficiency parameters can be grouped into three important and distinctive categories: reactor parameters, OSM properties, and operational parameters.

The *reactor parameters* include T_H, ε_G, ε_S, and $1/R_{\mathrm{TM}}$. These parameters are typically determined by the reactor design and are important to distinguish because they exhibit a monotonically increasing influence on the thermochemical conversion efficiency. Thus, an optimal reactor simply has maximum possible values for all reactor parameters, as limited by materials, cost or other feasibility issues. This relationship suggests that all reactors should strive to maximize T_H, ε_G and ε_S, and minimize R_{TM}. It should be noted, however, that the upper limit of T_H can be bounded by OSM stability.

The *OSM properties* include ΔH, ΔS, and C_P^{OSM}. These parameters are not as freely chosen as operational parameters. In theory, ΔH and ΔS could be optimized and C_P^{OSM} minimized to increase η. Although the tuning of ΔS and C_P^{OSM} have not received extensive attention, previous studies have shown that ΔH can be systematically tuned for certain materials (Scheffe and Steinfeld, 2012; Scheffe et al., 2013; Rormark et al., 2001; Mizusaki et al., 2000; Andersson et al., 2007; Yang et al., 2006; Dutta et al., 2006; Zhou et al., 2008; Gorte et al., 2006; Zhou et al., 2007). ΔH is therefore one of the most promising OSM material properties to explore with regards to improving reactor performance in the immediate future.

Finally, *operational parameters*, unlike reactor parameters, do not have monotonic relation to η and are expected to have optimal values, largely based on their coupling with the OSM properties. For a given set of reactor parameters and choice of OSM, P_{O_2}, T_L, and δ_O should be selected to maximize efficiency. For example, lowering P_{O_2} increases δ_R and increases the hydrogen produced per cycle, but requires escalating amounts of pump work due to low η_{Pump} at low pressures. Reducing δ_O increases the hydrogen production per cycle but also increases the water required for oxidation, because C_{H_2O} typically decreases as an OSM nears completion oxidation. Reducing T_L increases the thermal load of reheating the reactor and the OSM since it increases the temperature swing. However, it can also decrease δ_O (producing more hydrogen per cycle) or decrease the amount of water required for oxidation. For a given OSM, these relationships define a 3D design space $\eta(p_{O_2},\ T_L,\ \delta_O)$ which can be optimized to increase system efficiency through parametric study. It is also this 3D design space that defines the fundamental limitations on thermochemical conversion efficiency for two-step NRCs.

Grouping the parameters in this way is useful because it makes it clear how we can move towards the determination of the upper limiting efficiency for a given OSM. In the subsequent analysis we first examine the fundamental and practical limits on the reactor parameters, since they exhibit a monotonic effect on efficiency. Then we focus the remaining analysis on optimizing the operational parameters as a function of the OSM properties to determine the upper limiting efficiency for a given material. We then consider a variety of example cases to illustrate the relative importance of different reactor parameters for different OSM properties.

4.2. Fundamental and practical limits on reactor parameters

Mechanisms for solid phase heat exchange have been previously discussed (Ermanoski et al., 2013; Lapp and Lipiński, 2014), and improvements could significantly impact reactor performance. In order to reduce the energy load of preheating the water needed for oxidation, gas phase heat exchange can be used to recover sensible heat from the oxygen and hydrogen/water products of reaction steps one and two respectively. In a typical fluid heat exchanger, hot and cold fluids enter the heat exchanger at the inlets and flow past a solid wall that prevents chemical interaction/mixing between the two streams. Furthermore, this wall facilitates the exchange of sensible and/or latent heat. The effectiveness of a heat exchanger (ε_G) is directly related to the contact area, solid wall thermal conductivity and the convection coefficients of the fluids that exchange heat. The contact area is a function of the size and determines the capital cost of the heat exchanger. For gasses, the convection coefficient, while a function of many parameters, is strongly dependent on the density of the fluid. As a result, the heat exchangers needed to recover a significant portion of sensible heat in the gas phase products (e.g., O_2) from the reduction step will likely be limited by the low convection coefficient on the low pressure side. Such a heat exchanger is therefore likely to be large with low power density and, thus, expensive. Additionally, the impact on efficiency is minor due to the relatively small sensible heat carried by the O_2 gas stream (Ermanoski et al., 2013). The recovery of this sensible heat is therefore neglected from this analysis. Recovering the sensible heat of the water-hydrogen mixture produced in step two (OSM oxidation), on the other hand, is of particular importance when the OSM has a low C_{H_2O} value, and a value of 95% for ε_g has previously been used (Lapp et al., 2012; Ermanoski et al., 2013). Furthermore, it is critical to note that F_{Water} is fundamentally tied to the gas phase heat exchange efficiency (Eq. (9)). If ε_g were exactly 100%, F_{Water} would be zero. However $\varepsilon_g > 99\%$ will likely be cost prohibitive due to the size of the heat exchanger required to achieve it, which is a somewhat fundamental and practical limitation. Nonetheless, even taking the extremely high value of $\varepsilon_g = 99\%$ still would not change the qualitative conclusions that will be discussed later, specifically because as shown in Fig. 3, C_{H_2O} varies by many orders of magnitude. As a result, even in the best case, the energy penalty for preheating water is expected to be at least on the order of 1% of the energy required to heat n_{H_2O} from T^o to T_L. Since C_{H_2O} can easily change by orders of magnitude, even paying only 1% of this penalty can significantly impact efficiency when C_{H_2O} is very low, and the results of this study represent a lower limit for F_{Water}, which translates to an efficiency maximum.

One can establish the upper limit for efficiency by assuming the reactor is well-mixed with fast non-rate limiting reaction kinetics and follows reduction and oxidation paths similar to those shown in Fig. 2. Under these assumptions, the amount of water (n_{H_2O}) required to oxidize the OSM from δ_R to δ_O can be calculated using the path outlined in Fig. 2. After the OSM is reduced to δ_R, the temperature is lowered to T_L (Fig. 2 – location 4) and the OSM is then oxidized via exposure to steam (Fig. 2 – location 1). Assuming sufficiently fast kinetics, the equilibrium δ prescribed by Eq. (4) can be maintained at each P_{O_2} along the oxidation path (Fig. 2 – 4 → 1). Furthermore, if the reactor gases are well mixed and in equilibrium, then the P_{O_2} along this path is established by the ratio between the hydrogen generated and unreacted water vapor present in the reactor. Using Eq. (16), the percentage of water converted to hydrogen can then be found as a function of δ. In this manner, the water required for oxidation can be found by evaluating Eq. (18), and, in turn, the energy factor associated with preheating this water is found with Eq. (10).

While these assumptions give a conservative estimate of the energy required to preheat water for oxidation, such calculations indicate how reactor performance is truly impacted by different materials and how efficiency can be ultimately improved. In reality, the actual efficiency will be lower than this limiting case. However, relaxing these assumptions requires a more detailed description and analysis of the reactor that considers the finite kinetics of each reaction, as well as heat and mass transport limitations, as has been pursued by others (Yuan et al., 2015a,b; Keene et al., 2013; Lapp and Lipiński, 2014).

5. Results

5.1. Operational parameters for ceria, optimized reduction pressure

Incorporating the losses associated with incomplete conversion and pressure dependent pump efficiency not only change the expected efficiency, but also the optimum operating conditions. Consider a first example case of ceria as shown in Fig. 5, where different energy factors are sequentially included to illustrate their impact. Fig. 5 shows reference simulation data (Ermanoski et al., 2013) for efficiency vs. P_{O_2} along with predictions from the modelling framework introduced herein. For the conditions considered, the reference efficiency monotonically increases as P_{O_2} decreases (Fig. 5 – black line). If only F_{Reheat} and F_{RXN}

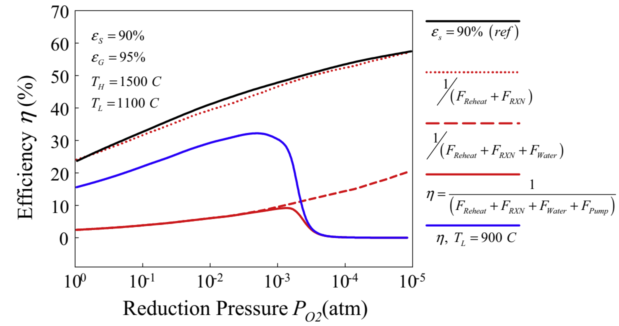

Fig. 5. Efficiency of ceria vs. P_{O_2} (Ermanoski et al., 2013). Reference efficiency, predicted efficiency, predicted efficiency neglecting certain energy factors, and efficiency when T_L is reduced to 900 °C ($\varepsilon_S = 90\%$, $\varepsilon_G = 95\%$, $T_H = 1500$ °C, $T_L = 1100$ °C, and $\delta_O = 0.001$).

are considered, as was the case for the reference data (Ermanoski et al., 2013), the efficiency predicted by the model presented herein (Fig. 5 – red[1] dotted line) matches the reference data with good agreement. However, even for an OSM with a large ΔH, such as ceria, if the energy required to preheat water is included, the efficiency reduces substantially, for the fixed oxidation temperature of 1100 °C (Fig. 5 – red dashed line) considered. Furthermore, if F_{Pump} is included, the monotonic relationship with decreasing P_{O_2} is lost and efficiency decreases significantly when the P_{O_2} becomes very low (Fig. 5 – solid red line). However, if the oxidation temperature is reduced to 900 °C, the overall efficiency more than doubles, because the decrease in F_{Water} overshadows the increase in F_{Reheat} (Fig. 5 – solid blue line). This initial example therefore shows how strongly the OSM properties and operational parameters are coupled and why one must optimize the operational parameters for a given OSM to determine its true potential for high efficiency.

To further understand how each operational parameter (T_L, P_{O_2}, and δ_O) impacts performance, energy factors for different conditions can be compared. In the ensuing analysis, the term optimized is used to indicate that one or several parameters were held constant as stated, but all other operational parameters were varied, to determine the maximum efficiency that could be achieved subject to the stated constraints. This approach then allows us to better understand the importance of certain parameters in certain regimes.

Fig. 6a shows the energy factors and efficiency vs. P_{O_2} of an optimized reactor. Of particular note is the effect of the pressure dependence of vacuum pump efficiency on reactor performance. Here, the efficiency reaches a maximum around $P_{O_2} = 10^{-3}$ atm. As P_{O_2} is reduced, the heat required to swing the temperature (Q_{Reheat}) remains constant, but δ_R increases (causing F_{Reheat} to decrease), thereby decreasing all energy factors other than F_{RXN}. As δ_R increases, more water is required to oxidize the OSM, but

[1] For interpretation of color in Fig. 5, the reader is referred to the web version of this article.

this additional water is used for oxidation when δ is large and C_{H_2O} is high. Therefore, the energy required to preheat this water increases slower than the energy output stored chemically, causing F_{Water} to decrease. For values of P_{O_2} above 10^{-3} atm, the pump efficiency ranges between 1% and 50% and F_{Pump} is small. However, at lower values of P_{O_2}, pump efficiency becomes very poor and F_{Pump} increases dramatically, which causes reactor performance to quickly decline.

Although not analyzed quantitatively in the present work, the combined use of a vacuum and inert sweep gas to achieve lower P_{O_2} and high η has been previously explored (Yuan et al., 2015a,b). Ermanoski et al. (2013) discussed how η is near zero for low P_{O_2} when a sweep gas is used, owing to the large amount of gas needed to reach very low P_{O_2}. They also reported a monotonic relationship between P_{O_2} and η using a vacuum pump, and concluded that combining a vacuum pump with an inert sweep gas is not a feasible approach for increasing η by reducing P_{O_2}. However, for a vacuum pump with pressure dependent performance, Fig. 6a shows a non-monotonic relationship between η and P_{O_2}. With pressure dependent pump efficiency there is a point of diminishing return and η decreases as P_{O_2} decreases further. This implies that the situation for a vacuum pump is similar of that of a sweep gas where an optimum P_{O_2} exists with a maximum η. Furthermore, the energetic expense of producing and preheating a fixed volume of inert gas decreases with total pressure due to the reduced gas density. Purging at a reduced total pressure could mitigate the energetic cost of an inert sweep gas, reducing the optimum P_{O_2} and increasing maximum efficiency. For such a system, initially a vacuum pump could be used to reduce the total pressure until pump efficiency became prohibitively small. Next, a sweep gas can be used at the low total pressure to further reduce P_{O_2} until further reduction exhibits diminishing returns on system efficiency. This approach has been analyzed by Yuan et al. and further suggests that significant gains can be obtained by combining the two approaches (Yuan et al., 2015a,b).

5.2. Optimization of the Oxidation Temperature and Extent of Oxidation

The effects of incomplete chemical conversion can be seen in Fig. 6b which shows reactor efficiency vs. δ_O. Even for ceria, complete oxidation at high temperatures requires large amounts of water and the efficiency suffers for δ_O below an optimum value. Additionally, the water required for oxidation increases further as ΔH of reduction decreases. This trend can be seen directly in Fig. 6c and d. Here, the efficiency is plotted vs. oxidation temperature for ceria (Fig. 6c) and a hypothetical OSM identical to ceria, with the exception that ΔH has been reduced by 15% (Fig. 6d). The optimum oxidation temperature for ceria is much higher than the OSM with a 15% lower ΔH, which can be understood through the conversion dependence (C_{H_2O}) on T_L (Fig. 3). Additionally, T_L appears in the limits of the integrals used to find F_{Reheat} and F_{Water} (Eqs. (8) and (10) respectively). In Fig. 6c and d, F_{Reheat} decreases as T_L increases, but eventually C_{H_2O} is so low that F_{Water} quickly increases presenting an effective wall for the efficiency. This situation prescribes an optimum T_L, which demonstrates why C_{H_2O} must be considered in NRC's. Nonetheless, the larger amount of hydrogen produced per cycle decreases all energy factors except F_{RXN}, making higher efficiencies still possible with a lower ΔH.

It is the analysis presented in Fig. 6 that identifies the limitations associated with chemical conversion and mechanical pumping efficiency as critical limitations on all thermochemical cycles of this type. Specifically, because the energy requirements for pumping and preheating act as a wall for the efficiency (see Fig. 6), these two effects have been deemed critical and they are fundamentally/practically insurmountable. Furthermore, this realization, that these effects ultimately limit the maximum efficiency for a given OSM, serves as one of the most important new insights derived from the present analysis.

6. Operational parameters for improved OSMs

6.1. Potential efficiency improvements with reduced ΔH

While some energetic penalties increase upon reducing ΔH, the overall reactor efficiency can increase if the operational parameters are optimized appropriately. Furthermore, both theoretical and experimental studies have shown that ceria alloys can exhibit lower ΔH of reduction (Scheffe and Steinfeld, 2012; Andersson et al., 2007; Yang et al., 2006; Dutta et al., 2006; Zhou et al., 2008; Gorte et al., 2006; Zhou et al., 2007). However, for actual materials, ΔH and ΔS can rarely be tuned independently (Zhou et al., 2007). Perovskite and ferrite oxides have also been demonstrated as viable OSM's with potentially lower values of ΔH (Scheffe et al., 2013, 2010; Rormark et al., 2001; Mizusaki et al., 2000), but whether or not these materials will lead to high efficiency in actual reactors remains undetermined.

Ceria is one of the few OSMs where the off-stoichiometry, ΔH, and ΔS have been determined for a wide range of applicable conditions (Panhans and Blumenthal, 1993; Zinkevich et al., 2006). This thermodynamic data is needed to build reactor models but requires extensive experimental characterization. This information does not typically exist for new materials, making it difficult to reliably predict their performance. While this paper has shown that material properties, including ΔH, ΔS, and C_P, impact reactor performance, methods for tuning ΔS and C_p of the OSM remain unclear. Additionally, these material properties are functions of δ and/or temperature and their functional dependencies differ from one material to the next. One promising approach to OSM design could

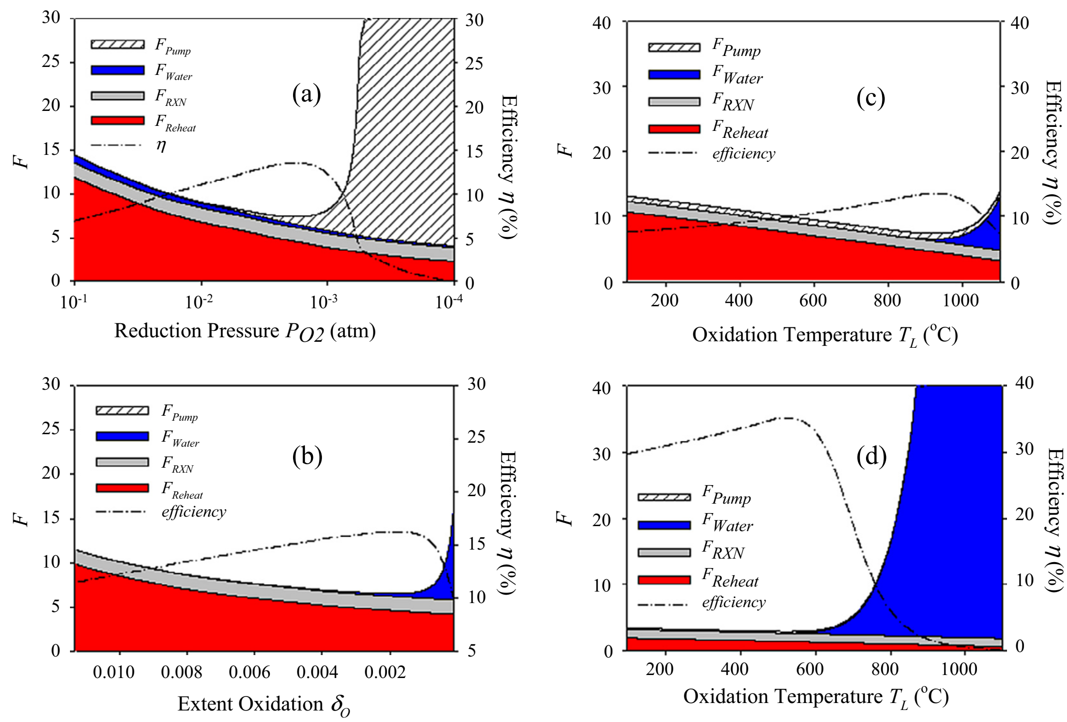

Fig. 6. Optimized efficiency and energy factors vs. various operating parameters for ceria (a–c) and (d) ceria with ΔH reduced by 15%. For operational parameters other than the specific one shown, all plots were created with optimized values. Values of $T_L = 950$ °C, $P_{O_2} = 0.0009$ (atm), and $\delta_O = 0.0023$ were used for plots a–c. Values of $\delta_O = 0.0023$ and $P_{O_2} = 0.0009$ (atm) were used for plot d.

involve not only modifying the values of these material properties, but also engineering their functional dependence on δ with the aim of improving NRC performance. Again, owing to the significant experimental effort required to fully characterize ΔH and ΔS as a function of T and δ for new materials, some initial approximations are needed to narrow the range of viable materials for such detailed characterization. However, to get a general sense, one could assume that new materials have a similar ΔS and C_P as ceria, as a first approximation. With these assumptions, the ΔH of ceria can be scaled and used to predict the efficiency improvements that can be achieved by lowering the value of ΔH, which may offer some insight into future directions for materials design/selection. By fixing ΔS and C_P at values corresponding to ceria and scaling ΔH, the maximum efficiency can be found by optimizing T_L, P_{O_2}, and δ_O. These results are shown in Fig. 7 for several combinations of ε_G and ε_S along with the maximum theoretical efficiency ($1/F_{\mathrm{RXN}}$) for a given ΔH.

In Fig. 7, a lower limit on oxidation temperature was imposed at T_L of 100 °C. Below this temperature, water condenses and while it is conceivable to split liquid water, the analysis must be modified which is beyond the scope of this work. Nonetheless, it may still be possible to split CO_2 or other oxygen-containing molecules of interest below 100 °C, although the oxygen mobility in the OSM decreases at reduced temperatures and the lower limit for T_L is likely to be above 100 °C. As expected, Fig. 7 shows that the optimized efficiency increases as ΔH decreases, and

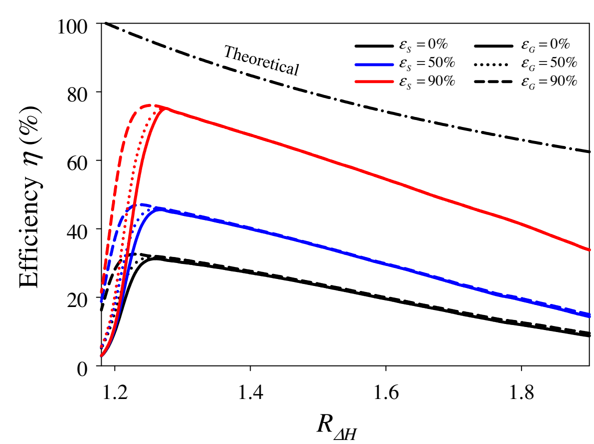

Fig. 7. Optimized maximum theoretical efficiency and maximum NRC efficiency vs. ΔH for nine different combinations of ε_S and ε_G values. Line color indicates ε_S and line style indicate ε_G according to the legend and the unstated parameters correspond to the values given in Table 1. ΔH is normalized to the enthalpy of water dissociation (241 kJ/mol H_2). The theoretical maximum efficiency for a given OSM is the inverse of F_{RXN}, and is 100% at $R_{\Delta H}$ of 1.2 because the ratio of the HHV_{H_2} to LHV_{H_2} is 1.2.

it is sensitive to ε_S but it is not sensitive to ε_G. Under optimized operational parameters and $T_L > 100$ °C, F_{Water} is relatively small (Fig. 6) and variations in ε_G have little impact. The reason that F_{Water} is small is that the optimum operating conditions occur shortly before encountering the dramatic (order of magnitude) increase in F_{Water} as δ_O is decreased. With 100 °C as a lower bound on oxidation temperature, for a very low value of ΔH, C_{H_2O} decreases but T_L cannot be further reduced to counteract the effects of poor conversion. With the inability to reduce T_L, the only way to oxidize the OSM is with excessive amounts of water and eventually F_{Water} becomes the dominating loss, reducing efficiency. Furthermore, because this reduction in efficiency is from F_{Water}, the point at which further reductions in ΔH decrease efficiency is moderately sensitive to ε_G. This sensitivity is observed in Fig. 7 where higher efficiency peaks are achieved with larger ε_G.

While all operational parameters are coupled, the optimum P_{O_2} is mainly governed by the η_{Pump}, ε_S, and ΔH, as shown in Fig. 8. For optimized operating conditions, as ε_S increases, F_{Reheat} decreases and F_{Pump} becomes a higher portion of the denominator of Eq. (7). As F_{Reheat} decreases, P_{O_2} must increase to reduce F_{Pump} in order to reach the highest possible efficiency.

Fig. 9 shows the largest and smallest values of optimal T_L for all combinations of ε_S and ε_G considered. Here, the optimal T_L increases as ΔH increases, because materials with large values of ΔH have high C_{H_2O}. Furthermore, optimal T_L increases as ε_G increases, because the energetic penalty for preheating unreacted water is small when ε_G is high. On the other hand, for high values of ε_S, the energetic expense of heating from T_L to T_H decreases, reducing optimum T_L. When $\varepsilon_S = 0$ and $\varepsilon_G = 90\%$, the minimum temperature is never reached because F_{Reheat} is nearly equal to the sum of all other energy factors when $R_{\Delta H}$ is low. Therefore, further reductions in temperature would reduce efficiency more than using large amounts of water for oxidation.

In all cases, the optimum value of ΔH is higher than the enthalpy of water dissociation (~241 kJ/mol H_2). In Fig. 9, the optimum value of ΔH is more than 20% above the enthalpy of water dissociation. For values of $R_{\Delta H}$ below 1.2, C_{H_2O} becomes very small and the large amounts of water required for oxidation decrease the efficiency. While low temperature oxidation has been demonstrated (Singh and Hegde, 2009) for nanomaterials, oxidation kinetics could become prohibitively slow even at higher temperatures (Chueh and Haile, 2009) for OSMs with larger grains/pore sizes (i.e., an OSM that may exhibit higher temperature stability and cycle durability). Such slow kinetics, can lead to long reaction times and increased F_{Loss}. If the lower limit for T_L is restricted to temperatures around 400 °C, then the optimum value of $R_{\Delta H}$ increases to almost 1.4.

Fig. 10 shows the largest and smallest averaged C_{H_2O} values for all combinations of ε_S and ε_G considered. For similar reasons, the relative values of these curves are similar to the values of T_L in Fig. 9. All average C_{H_2O} values decrease sharply after T_L reaches its minimum value. Additionally, for $R_{\Delta H}$ above 1.3, the minimum value of the averaged C_{H_2O} is always above ~3.55%. This indicates that NRC efficiency will certainly be low for materials where the water required for oxidation is greater than 100 times the hydrogen produced.

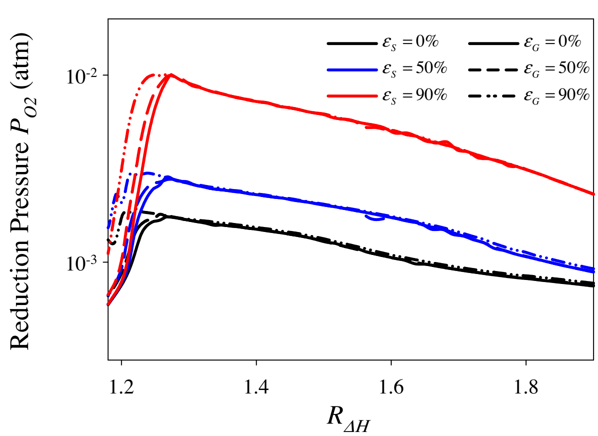

Fig. 8. Optimized P_{O_2} vs. ΔH for nine different combinations of ε_S and ε_G values. Line color indicates ε_S and line style indicate ε_G according to the legend and the unstated parameters correspond to the values given in Table 1. ΔH is normalized to the enthalpy of water dissociation (241 kJ/mol H_2).

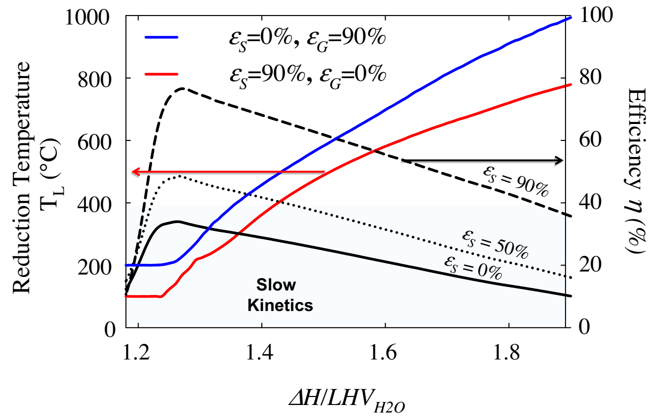

Fig. 9. Maximum and minimum of T_L for all combinations of ε_S and ε_G considered. Average optimized efficiency vs. ΔH for $\varepsilon_S = 0\%$, 50%, and 90% respectively. ΔH is normalized to the enthalpy of water dissociation (approximately 241 kJ/mol H_2).

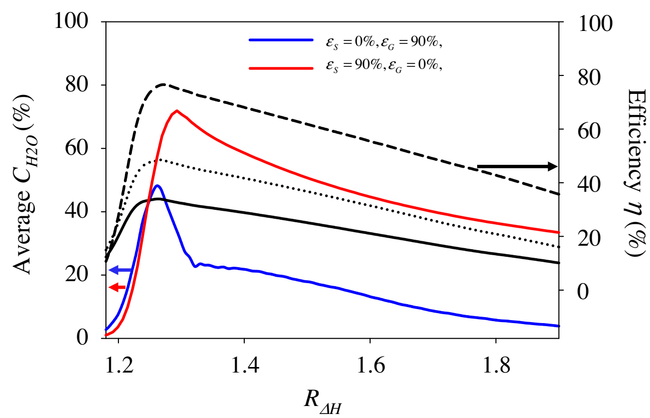

Fig. 10. Maximum and minimum of average C_{H_2O} for all combinations of ε_S and ε_G considered. Average optimized efficiency vs. ΔH for $\varepsilon_S = 0\%$, 50%, and 90% respectively. ΔH is normalized to the enthalpy of water dissociation (241 kJ/mol H_2).

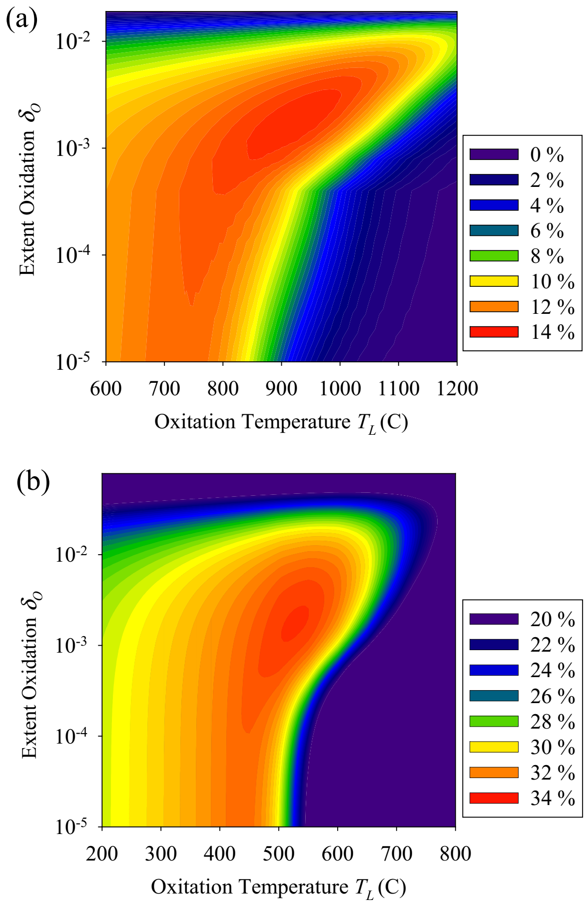

Fig. 11. Plots of δ_O vs. T_L revealing efficiency (η) profiles for (a) ceria and (b) a ceria-like material with a 15% lower ΔH of reduction with $\varepsilon_S = 0.9$ and $\varepsilon_G = 0.5$. Note: that the temperature axes on (a) and (b) are different illustrating that the optimum oxidation temperature for a material with lower ΔH occurs at a lower temperature. The shallow maximum is shown by the constant, maximum efficiency over a wide range of values for T_L.

6.2. Trade-offs between T_L and δ_O

Due to the energetic trade-offs between oxidizing at lower temperature with high C_{H_2O} and oxidizing at higher temperature with low C_{H_2O}, NRC efficiency has a very shallow maximum with respect to T_L and δ_O. These shallow maxima indicate that many different combinations of these two parameters can give a similar, near maximum efficiency. This can be seen in Fig. 11 for two values of ΔH and optimized operational parameters. For higher values of ΔH (Fig. 11a), when the oxidation temperature is low (<900 °C), high efficiency is achieved by oxidizing the OSM closer to completion (i.e. at relatively low values of δ_O). However, at higher oxidation temperatures, large amounts of water are required to oxidize the OSM and the efficiency peaks further away from complete oxidation (i.e. at relatively large values of δo). For a lower value of ΔH (Fig. 11b), a low C_{H_2O} reduces the range of T_L with near maximum efficiency, and near maximum efficiencies are not possible for low values of δ_O.

For a given material, the oxidation temperature (T_L) can be selected from a range of temperatures defined by this shallow maximum all of which have nearly the same efficiency (between 800 °C and 1000 °C in Fig. 11a). Faster oxidation reaction kinetics generally occur at higher temperatures, motivating higher value of T_L. However, increasing T_L increases the average temperature of the reactor, increasing $\dot{Q}_{Loss}$. For high values of ΔH, where T_L can be selected from a range of values, optimum values should likely be selected from a more detailed analysis which considers the competition between reaction kinetics and heat leakage.

6.3. Maximizing system efficiency requires simultaneous optimization of OSM and reactor parameters

It should be emphasized that the quantitative results shown here are a direct result of the values in Table 1 and will change for different reactor parameters, such as T_H, pump efficiency, and OSM properties ($\Delta H(\delta)$, $\Delta S(\delta)$, and C_P). However the underlying physics and qualitative relationships governing these results are not expected to change dramatically, as the major innovation here is the new method. Pump efficiency is a function of P_{O_2}, and lower limits for P_{O_2} come from this dependence. Materials with low values of ΔH will also have low values of C_{H_2O}. Furthermore, in combination with lower limits on T_L (likely due to kinetics), ε_G and C_{H_2O} establish a lower

Table 1
Default model parameters, unless otherwise specified.

Percent solid phase heat recovery	ε_S	50%
Percent gas phase heat recovery	ε_G	90%
Reduction temperature	T_H	1500 °C
Ratio of inert reactor thermal mass to OSM thermal mass	R_{TM}	0
Pump efficiency	η_{Pump}	Fig. 4
Specific heat of OSM (ceria)	C_p^{OSM}	Aguileragranja and Moranlopez (1993)
Specific heat of water	$C_p^{H_2O}$	Çengel and Boles (2006)
Reduction enthalpy	$\Delta H(\delta)$	470 kJ/mol H_2[a] Panhans and Blumenthal (1993)
Reduction entropy	$\Delta S(\delta)$	260 J/mol H_2[a] Panhans and Blumenthal (1993)

[*] Value represents an average evaluated at typical operating conditions although a complete function of δ was actually used.

limit for ΔH. This lower limiting value of ΔH is likely to be greater than the enthalpy of water dissociation around $\Delta H/\Delta H_{H_2O} \sim 1.4$.

Furthermore, the importance of reactor design should be emphasized. While the operational parameters and ΔH define a highly coupled design space, T_R, ε_G, ε_S, and R_{TM} are also likely coupled through reactor geometry and operational conditions. As an example, Lapp and Lipiński (2014) discussed a reactor where ε_S depends on the difference between T_H and T_L (further motivating the operation of the reactor at the highest T_L of the shallow maximum with near maximum efficiency for a given value of ΔH). A more thorough analysis would account for this dependence and is likely specific to a given reactor design/concept. Other considerations include the coupling of ε_S and the ratio of inert reactor thermal mass to OSM thermal mass (R_{TM}) which appears as a coefficient in F_{Reheat} (Eq. (8)). A well designed reactor should minimize this ratio, similar to a packed bed reactor where none of the inert reactor material experiences the temperature swing between T_H and T_L. For other reactor designs where this ratio is not small, Eq. (8) shows the important parameter to minimize is $(1-\varepsilon_S)(R_{TM}+1)$.

From the results in Fig. 7, it can be seen that ΔH and $(1-\varepsilon_S)(R_{TM}+1)$ are of roughly equal importance for achieving high efficiency in NRC's. Siegel et al. (2013) reported that thermochemical conversion efficiency must exceed 30% to be competitive with solar driven electrolysis. Even for the conditions analyzed here, this metric is possible but will likely require improved OSM's. For ceria ($\Delta H/\Delta H_{H_2O} \approx 1.95$), more than 50% solid phase heat recovery is required to exceed NRC efficiencies of 30%, but with modest reductions in ΔH, η larger than 30% are possible for ε_S less than 50%. Therefore the most promising approach involves modest improvements in both reactors and OSM's. Furthermore, because the optimum ΔH is only a weak function of ε_S and ε_G, the work to improve reactor design and engineer new OSMs can proceed somewhat independently, except for issues associated with materials compatibility.

For reactors with an OSM and reduction temperature that requires a low P_{O_2} to achieve high δ, a vacuum pump has been commonly suggested as the method of choice for achieving a low P_{O_2}. With constant pump efficiency, F_{Pump} is small relative to other energy factors and efficiency monotonically increases as P_{O_2} decreases. However, as shown herein, mechanical pumping efficiencies are not constant and are highly sensitive to reduction pressure. Furthermore, this efficiency is extremely low at lower pressures due to reduced molecular flow rates from low gas densities and a constant frictional loss. While better pumps optimized for thermochemical cycles may be possible, flow and efficiency is still pressure dependent and this dependence in combination with ε_s defines the optimum P_{O_2} for high performance. For the pumps considered, the high losses that accrue from pumping large volumes of O_2 at low pressure render the use of vacuum pumps alone impractical for operating at reduction pressures less than $\sim 10^{-3}$ atm. This is important, because most OSM testing has focused on operating at pressures in the range of 10^{-5}–10^{-6} atm. Additionally, the turbo pump shown in Fig. 4 is considered a highly energy efficient pump for high vacuum as this technology is commonly used in semiconductor manufacturing, an industry where achieving a high vacuum efficiently is an economic driver.

Implementing new OSM's with low values of ΔH allows greater oxygen off-stoichiometry to be achieved during reduction which, in turn, may increase efficiency. As a result, discovering advanced OSMs is one of the most promising ways to increase system efficiency. Many analyses assume 100% water to hydrogen conversion or small or fixed losses from incomplete conversion (such as 3%) Siegel et al., 2013; Ermanoski et al., 2013. While this assumption is valid for ceria (an OSM with high conversion), lowering ΔH reduces the extent of conversion. Thus, when evaluating new materials with lower values of ΔH or when oxidizing at a high T_L, the impact of such parameters on F_{Water} must be considered in efficiency calculations.

Lower values of ΔH lead to higher fuel production per cycle but also lower conversion (increasing F_{Water}). These opposing effects suggest that for a given OSM, there are optimum operational parameters that are highly dependent on T_L. For T_L as low as 100 °C and a material similar to ceria, the optimum value of ΔH of reduction is greater than the enthalpy change for water dissociation by a factor of $\sim$1.2.

Conclusions

A new framework for assessing the maximum efficiency that a two-step partial redox cycle can achieve with a certain OSM has been presented. The model relies on limiting conservative assumptions and identifies qualitative trends in how an optimized reactor would be operated for different OSMs, some of which are non-obvious. The modelling framework includes the penalties associated with using a vacuum pump to reduce the oxygen partial pressure during the reduction step and it also includes the penalty associated with incomplete conversion (e.g., the need to supply excess reactant to drive the oxidation reaction). These two issues lead to important and critical limitations on the maximum efficiency that can be obtained for a given OSM and allow for identification of the optimal OSMs characteristics. Many studies compare new OSMs to ceria as an evaluation metric by measuring the hydrogen produced per cycle under a common reduction P_{O_2}, a common reduction temperature, and with very large amounts water during oxidation. While this method serves as a quick method for screening materials as viable OSMs, deeper reduction may not lead to higher efficiencies, because optimum efficiency can occur at different values of P_{O_2} and T_L for different materials. An OSM that produces more H_2

than ceria will not necessarily achieve higher efficiencies in a real reactor. For example, ceria can be oxidized at a high temperature and even though less H_2 may be produced with ceria, F_{Reheat} is smaller than that of an OSM with a lower value of ΔH, so it is possible that the overall efficiency could still be higher for ceria. We assert that a model such as the one described herein should be used to estimate the maximum NRC efficiencies possible, taking as inputs selected reactor parameters and data describing $\Delta H(\delta)$ and $\Delta S(\delta)$ for new OSMs. This would allow one to predict limiting efficiencies, and compare candidate OSMs on an equal footing.

Acknowledgement

This work was conducted under the financial support of ARPA-E project DE-AR0000339.

Appendix A. Supplementary material

Supplementary data associated with this article can be found, in the online version, at http://dx.doi.org/10.1016/j.solener.2015.09.036.

References

Abanades, S. et al., 2006. Screening of water-splitting thermochemical cycles potentially attractive for hydrogen production by concentrated solar energy. Energy 31 (14), 2805–2822.

Aguileragranja, F., Moranlopez, J.L., 1993. Specific-heat and the phase-diagram of the ising square lattice with nearest-(Ji) and next-nearest interactions. J. Phys.-Condens. Matter 5, A195–A196.

Aleklett, K. et al., 2010. The peak of the oil age – analyzing the world oil production reference scenario in world energy outlook 2008. Energy Policy 38 (3), 1398–1414.

Andersson, D.A. et al., 2007. Modeling of CeO_2, Ce_2O_3, and CeO_{2-x} in the LDA plus U formalism. Phys. Rev. B 75 (3).

Bader, R. et al., 2013. Thermodynamic analysis of isothermal redox cycling of ceria for solar fuel production. Energy Fuels 27 (9), 5533–5544.

Bader, R. et al., 2013. Solar syngas production via isothermal nonstoichiometric redox cycling of ceria with heat recovery. Abstr. Pap. Am. Chem. Soc. 245.

Brendelberger, S., et al., 2014. Solid phase heat recovery and multi chamber reduction for redox cycles. In: ASME 2014 8th International Conference on Energy Sustainability collocated with the ASME 2014 12th International Conference on Fuel Cell Science, Engineering and Technology. 2014. American Society of Mechanical Engineers.

Bulfin, B. et al., 2015. Thermodynamics of CeO_2 thermochemical fuel production. Energy Fuels 29 (2), 1001–1009.

Çengel, Y.A., Boles, M.A., 2006. Thermodynamics: An Engineering Approach. McGraw-Hill Higher Education.

Chaisson, E.J., 2008. Long-term global heating from energy usage. Eos, Trans. Am. Geophys. Union 89 (28), 253–254.

Chueh, W.C., Haile, S.M., 1923. A thermochemical study of ceria: exploiting an old material for new modes of energy conversion and CO_2 mitigation. Philos. Trans. R. Soc., A 2010 (368), 3269–3294.

Chueh, W.C., Haile, S.M., 2009. Ceria as a thermochemical reaction medium for selectively generating syngas or methane from H_2O and CO_2. Chemsuschem 2 (8), 735–739.

Dutta, G. et al., 2006. Origin of enhanced reducibility/oxygen storage capacity of $Ce_{1-x}Ti_xO_2$ compared to CeO_2 or TiO_2. Chem. Mater. 18 (14), 3249–3256.

Ermanoski, I., Siegel, N.P., Stechel, E.B., 2013. A new reactor concept for efficient solar-thermochemical fuel production. J. Sol. Energy Eng.-Trans. ASME 135 (3).

Ermanoski, I., Miller, J., Allendorf, M., 2014. Efficiency maximization in solar-thermochemical fuel production: challenging the concept of isothermal water splitting. Phys. Chem. Chem. Phys. 16 (18), 8418–8427.

Funk, J.E., 2001. Thermochemical hydrogen production: past and present. Int. J. Hydrogen Energy 26 (3), 185–190.

Funk, J.E., Reinstro, R.M., nk and Reinstro 1966. Energy requirements in production of hydrogen from water. Ind. Eng. Chem. Process Design Dev. 5 (3), 336–342.

Furler, P. et al., 2013. Solar thermochemical CO_2 splitting utilizing a reticulated porous ceria redox system. Energy Fuels 26 (11), 7051–7059.

Gleckman, P., O'Gallagher, J., Winston, R., 1989. Concentration of sunlight to solar-surface levels using non-imaging optics. Nature 339 (6221), 198–200.

Gorte, R.J. et al., 2006. Thermodynamic investigation of the redox properties of ceria-zirconia solid solutions. Abstr. Pap. Am. Chem. Soc. 231.

Holladay, J.D. et al., 2009. An overview of hydrogen production technologies. Catal. Today 139 (4), 244–260.

IEA's World Energy Outlook, 2013.

Keene, D.J., Davidson, J.H., Lipinski, W., 2013. A model of transient heat and mass transfer in a heterogeneous medium of ceria undergoing nonstoichiometric reduction. J. Heat Transfer-Trans. ASME 135 (5).

Keene, D.J., Davidson, J.H., Lipiński, W., 2013. A model of transient heat and mass transfer in a heterogeneous medium of ceria undergoing nonstoichiometric reduction. J. Heat Transfer 135 (5), 052701–052701.

Koepf, E. et al., 2012. A novel beam-down, gravity-fed, solar thermochemical receiver/reactor for direct solid particle decomposition: design, modeling, and experimentation. Int. J. Hydrogen Energy 37 (22), 16871–16887.

Krenzke, P.T., Davidson, J.H., 2015. On the efficiency of solar H_2 and CO production via the thermochemical cerium oxide redox cycle: the option of inert-swept reduction. Energy Fuels 29 (2), 1045–1054.

Lange, M. et al., 2014. T–S diagram efficiency analysis of two-step thermochemical cycles for solar water splitting under various process conditions. Energy 67, 298–308.

Lapp, J., Lipiński, W., 2014. Transient three-dimensional heat transfer model of a solar thermochemical reactor for H_2O and CO_2 splitting via nonstoichiometric ceria redox cycling. J. Sol. Energy Eng. 136 (3).

Lapp, J., Davidson, J.H., Lipinski, W., 2012. Efficiency of two-step solar thermochemical non-stoichiometric redox cycles with heat recovery. Energy 37 (1), 591–600.

Loutzenhiser, P.G., Steinfeld, A., 2011. Solar syngas production from CO_2 and H_2O in a two-step thermochemical cycle via Zn/ZnO redox reactions: thermodynamic cycle analysis. Int. J. Hydrogen Energy 36 (19), 12141–12147.

Mallapragada, D.S., Agrawal, R., 2014. Limiting and achievable efficiencies for solar thermal hydrogen production. Int. J. Hydrogen Energy 39 (1), 62–75.

McDaniel, A.H. et al., 2013. Sr and Mn doped $LaAlO_3$-d for solar thermochemical H_2 and CO production. Energy Environ. Sci. 6 (8), 2424–2428.

McDaniel, A.H. et al., 2013. Sr- and Mn-doped $LaAlO_3$-delta for solar thermochemical H-2 and CO production. Energy Environ. Sci. 6 (8), 2424–2428.

Meredig, B., Wolverton, C., 2011. First-principles thermodynamic framework for the evaluation of thermochemical H_2O- or CO_2-splitting materials (vol 80, 245119 2009). Phys. Rev. B 83 (23).

Miller, J.E., McDaniel, A.H., Allendorf, M.D., 2014. Considerations in the design of materials for solar-driven fuel production using metal-oxide thermochemical cycles. Adv. Energy Mater. 4 (2).

Mizusaki, J. et al., 2000. Oxygen nonstoichiometry and defect equilibrium in the perovskite-type oxides $La_{1-x}Sr_xMnO_{3+d}$. Solid State Ionics 129 (1–4), 163–177.

Muhich, C.L. et al., 2013. Efficient generation of H_2 by splitting water with an isothermal redox cycle. Science 341 (6145), 540–542.

Ngoh, S.K., Njomo, D., 2012. An overview of hydrogen gas production from solar energy. Renew. Sustain. Energy Rev. 16 (9), 6782–6792.

Panhans, M.A., Blumenthal, R.N., 1993. A thermodynamic and electrical-conductivity study of nonstoichiometric cerium dioxide. Solid State Ionics 60 (4), 279–298.

Rormark, L. et al., 2001. Enthalpies of oxidation of CaMnO3-d, Ca2MnO4-dand SrMnO3-d – deduced redox properties. Chem. Mater. 13 (11), 4005–4013.

Scheffe, J.R., Steinfeld, A., 2012. Thermodynamic analysis of cerium-based oxides for solar thermochemical fuel production. Energy Fuels 26 (3), 1928–1936.

Scheffe, J.R., Li, J.H., Weimer, A.W., 2010. A spinel ferrite/hercynite water-splitting redox cycle. Int. J. Hydrogen Energy 35 (8), 3333–3340.

Scheffe, J.R., Weibel, D., Steinfed, A., 2013. Lanthanum-strontium-manganese perovskites as redox materials for solar thermochemical splitting of H_2O and CO_2. Energy Fuels 27 (8), 4250–4257.

Siegel, N.P. et al., 2013. Factors affecting the efficiency of solar driven metal oxide thermochemical cycles. Ind. Eng. Chem. Res. 52 (9), 3276–3286.

Singh, P., Hegde, M.S., 2009. $Ce_{0.67}Cr_{0.33}O_{2.11}$: a new low-temperature O_2 evolution material and H_2 generation catalyst by thermochemical splitting of water. Chem. Mater. 22 (3), 762–768.

Steinfeld, A., 2005. Solar thermochemical production of hydrogen – a review. Sol. Energy 78 (5), 603–615.

Venstrom, L.J. et al., 2014. Efficient splitting of CO_2 in an isothermal redox cycle based on ceria. Energy Fuels 28 (4), 2732–2742.

Yang, Z., Woo, T.K., Hermansson, K., 2006. Effects of Zr doping on stoichiometric and reduced ceria: a first-principles study. J. Chem. Phys. 124 (22).

Yuan, C. et al., 2015a. A new solar fuels reactor concept based on a liquid metal heat transfer fluid: reactor design and efficiency estimation. Sol. Energy 122, 547–561.

Yuan, C. et al., 2015b. A new solar fuels reactor using a liquid metal heat transfer fluid: modeling and sensitivity analysis. J. Therm. Eng., in press.

Zhou, G. et al., 2007. Oxidation entropies and enthalpies of ceria-zirconia solid solutions. Catal. Today 123 (1–4), 86–93.

Zhou, G., Hanson, J., Gorte, R.J., 2008. A thermodynamic investigation of the redox properties of ceria-titania mixed oxides. Appl. Catal. A-General 335 (2), 153–158.

Zinkevich, M., Djurovic, D., Aldinger, F., 2006. Thermodynamic modelling of the cerium-oxygen system. Solid State Ionics 177 (11–12), 989–1001.